Egyptian Journal of Chemistry
http://ejchem.journals.ekb.eg/

Enhancement of The Performance of Dye-sensitized Solar Cells Using Sensitized Zinc Oxide Nanoparticles by Rhodamine B dye

Hussam Musleh[1,2,*], Hamdia Zayed[2], Samy Shaat[3], Amal Al-Kahlout[1], Hassan Tamous[4], Ahmed Issa[5], Jehad Asad[1] and Naji AlDahoudi[1]

[1]*Al Azhar University-Gaza, Physics Department, Gaza, Palestine.*
[2]*Ain Shams University, Women's College for Arts, Science, and Education, Physics Department, Cairo, Egypt.*
[3]*Islamic University of Gaza, Physics Department, Gaza, Palestine.*
[4]*Al Azhar University-Gaza, Chemistry Department, Gaza, Palestine.*
[5]*Al Azhar University-Gaza, Faculty of Engineering and IT, Department of Engineering, Gaza, Palestine.*

IN THE PRESENT work, ZnO nanoparticles were synthesized via a simple wet chemical (hydrothermal) technique using zinc acetate dihydrate ($Zn(CH_3COO)_2.2H_2O$) as a row material dissolved into absolute methanol and aqueous NaOH as precipitation agent. The X-ray diffractometer (XRD) patterns showed a standard hexagonal wurtzite structure of ZnO NPs with average particle size of about 28±2 nm. High resolution-transmission electron microscopy (HR-TEM) micrograph of ZnO NPs showed semi-spherical particles with an average size of about 25.3±6 nm, which agreed well with the XRD results. UV-Vis spectrum of the ZnO NPs revealed the highest absorption band at 366.4 nm and the optical energy gap (E_g) was about 3.12 eV. The Photoluminescence spectrophotometer (PL) spectrum emission illustrated lower UV emission than the visible emission. This indicated to the high defect density in ZnO sample. The effect of concentration of cost-effective Rhodamine B dye on the performance of dye-sensitized solar cells) DSSCs) based on ZnO NPs has been studied. The best performance among the five concentrations was 0.7 mM. The photon to electric energy conversion efficiency of the DSSCs has been found to increase by eight times from 0.07 to 0.58 %. Transient open-circuit voltage decay (TOCVD) method has been used to investigate the electron lifetime (τn) and the electron recombination velocity (K_{rec}) in DSSCs, by using the double exponential function. The results revealed that the Rhodamine B dye can be an efficient dye as a low-cost sensitizing dye for DSSCs.

Keywords: ZnO NPs, Hydrothermal, PL, Rhodamine B and DSSCs.

Introduction

Recently, ZnO NP have become one of the most important metal oxide (MO) which used as a semiconductor material that has a wide and direct optical band gap about 3.37 eV as well as a large exciton binding energy at room temperature (about 60 meV) [1, 2]. This leads to attractive properties in electronic and opto-electronic applications such as, solar cells [3], gas sensors[4] and photoemitters [5]. In addition, ZnO is a non-toxic material. This means it has may application in bio medication such as, fluorescence imaging which has been extensively used in preclinical examination[6] and textiles finishing [7]. In addition, zinc ion is a vital trace element for adults and it is involved in various aspects of metabolism. In the United States, about 11.0 mg and 9.0 mg of zinc ions/day is recommended for adult males and females, respectively [6].There are two main approaches of synthesis MO NPs (mainly ZnO NPs). Physical and wet chemical techniques have been reported in many literatures. Physical techniques includes radio frequency magnetron sputtering (RFMS)[8], laser deposition [9], molecular beam epitaxy (MBE)[10, 11]. On

*Corresponding author e-mail: h.mphysics@hotmail.com
Received 28/2/2019; Accepted 14/5/2019
DOI: 10.21608/ejchem.2019.12677.1785

the other hand, chemical techniques include co-precipitation[12], hydrothermal [13], sol gel [14] and others. Wet chemical method has been chosen because of simplicity, economical consideration and highly efficient of the process[15]. In addition, the capability to control the particle size and morphology is more available over other methods to optimize the properties of NPs by adjusting the influence of parameters such as solvent [16], metal source precursor salts (nitrate, acetate, chlorate, sulfate)[17], molar ratio[18], pH value[19], calcination temperature[10], aging time[20], the presence of additives surfactant or polymer[21] and any other metal doping[22]. Until now, hydrothermal technique of zinc salt such as ($Zn(CH_3COO)_2.2H_2O$) is still a commanding technique to obtain ZnO NPs. Zinc acetate dihydrate precursor has a high solubility and low decomposition temperature so it is often chosen as a powerful precursor[20,23,24].

In this paper, ZnO NPs were synthesized via hydrothermal technique for use as a photoanode of dye sensitized solar cells (DSSCs). The structural and optical properties of the synthesized, ZnO NPs were studied. Different concentration of low-cost chemical dye named Rhodamine B ($C_{28}H_{31}Na_2O_3Cl$) from xanthene derivatives, Mw = 479.02 g/mole, were dissolved in ethanolic solution. Dye was characterized by UV-Vis absorption spectroscopy.

The photovoltaic properties of the fabricated DSSCs were investigated using J-V characteristics curve. When compared with other organic dyes, Rhodamine B was used as a photosensitizer, which is thousand times cheaper than the Ru-based dye. In addition, it is easier to recycle metal-free dye-based cells [25]. Our ongoing work enhances the anchoring between semiconductor surface (ZnO or TiO_2) and dye branches based on the modification of Rhodamine B dye by adding some functional groups. This leads to enhance the performance of the harvesting and electron injection of such dyes.

Materials and Methods

Materials

All chemicals used were of analytical reagent grade (AR) and of highest purity available. Zinc acetate dihydrate, $Zn(CH_3COO)_2.2H_2O$ (ZA), sodium hydroxide (NaOH) ≥ 98.9% was purchased from Merck and absolute methanol, (CH4O) ≥ 99 % was purchased from SDFCL.

Preparation of ZnO NPs

Hydrothermal route was used to synthesize pure ZnO NPs. 4.0 g of ZA was dissolved in 50 ml of pure methanol. After vigorous stirring for 30 min at a temperature of 60 °C and sonication for 30 min, a colorless homogenous solution was obtained. Drops of 5M aqueous NaOH solution was added drop wise to zinc acetate solution under vigorous stirring at 60 °C until pH about 14. The colorless homogenous solution changed to milky white slurry colloidal. The white colloidal was stirred for 1hr at a temperature of 60 °C. The colloidal was transferred to 100 ml Teflon lined stainless steel autoclave for 3hr at a temperature of 160 °C. After that, a white precipitate was, carefully, collected and then, centrifuged at 3500 rpm by washing 5 times for 90 min with absolute ethanol to remove the debris, the excessive salts and the leftover unreacted materials. Finally, the residual product was left to dry overnight at a temperature of 120 °C, and then, crushed into fine powder form. Fig.1 shows the procedure for the preparation of ZnO NPs using hydrothermal technique.

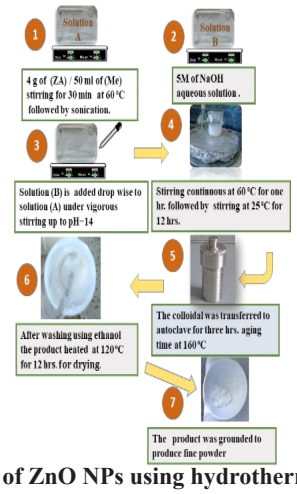

Fig. 1. Flowchart for the preparation of ZnO NPs using hydrothermal technique.

Fabricate and assembly of the DSSCs devices

Synthesized ZnO NPs powder, were used as semiconductor electrodes. The slurry past was prepared by mixing 0.06g of ZnO NPs, 6 drops of polyethylene glycol (400) (PEG 400) and 10 drops of absolute ethanol by using a mortar and pestle for 12 min. The paste was deposited on the conductive side of fluorine-doped SnO_2 (FTO). Conducting glass was supported by adhesive tape to define the active area. The layer was dried at 120°C for 20 min followed by sintering at 450°C for 40 min in air. The surface area was about 0.5×0.5 cm^2 and the thickness of the obtained sintered layer was lied between 12 to 15µm. The prepared films of ZnO NPs photoanode immersed separately in different concentrations solutions of 0.1, 0.3, 0.5, 0.7 and 1 mM, of RB dye to sensitize them for 12 hr.

After that, the films were rinsed in absolute ethanol and were dried naturally. A Pt-coated FTO substrate was used as the counter electrode.

A redox, (I^-/I^{-3}) electrolyte solution was prepared by dissolving 0.334 g of LiI, and 0.0317 g of I_2 in 4 mL of propylene carbonate and 1mL of acetonitrile. Electrolyte was injected between photoanode and counter electrode to filling the space between them.

To measure the adsorbed dye amount on the coloured films, the photoanode was immersing in a 0.1M NaOH solution of water and ethanol (1:1, v/v). UV-Vis spectrophotometer was employed to measure the dye concentration of the desorbed-dye solution as described in previous work [25].

The transient open circuit photovoltage (TOCPV) decay experiment is conducted by monitoring the subsequent decay of TOCPV due to turning off the light source after illuminating the DSSCs devices based the of 0.7mM RB dye for 5 minutes.

Characterization Measurements

The chemical compositions were examined using an energy dispersive X-ray analyzer (EDX) coupled to a scanning electron microscope (Philips-Quanta FEG 250).

The crystal identification and crystal size analysis of the powder were examined by X- ray diffractometer (XRD), Philips Expert, where Cu-Kα radiation (λ=1.5418 Å) monochromated by a nickel filter. Diffraction angle (2θ) values ranging from 15˚ to 80°. The nanostructures and their lattice images were taken with a 200 kV high-resolution transmission electron microscopy (HRTEM) (JEM-2100), 200 kV. Double beam UV-vis spectrophotometer (Shimadzu UV-1601 PC) was used to carry out the absorption spectra of synthesized powder and the absorption of sensitizing dye in the range from 300 nm to 800 nm in ethanolic solutions. Photoluminescence (PL) emission measurements were carried out at room temperature in absolute ethanol with (SPF-200 (Biotech Engineering Management Co., UK) spectrofluorometer in the range from 300 nm to 800 nm with excitation wavelength 320 nm. The photovoltaic characteristics of the fabricated solar cell samples were investigated using the current density against voltage (J–V) characteristic curves under focusing irradiation with white light from a 40W Xenon arc lamp in ambient atmosphere. Using a personal computer connected with Elvis National Instruments (ENI) in combination with a LabVIEW program. The illumination light intensity was about 100 $mWcm^{-2}$. The characteristic curves of the fabricated cells were excused by applying an external reverse bias voltage in the range -1 to 1V of the solar cell.

Results and Discussion

EDX Analysis

EDX technique is used for identifying the chemical composition of the prepared sample. The higher a peak, indicates that high concentrated element in the tested sample. An EDX spectrum plot identifies the element corresponding to each of its peaks, and the type of X-ray to which it corresponds as well. The EDX analysis of the prepared ZnO sample is depicted in Fig. 2. In addition, Zn and O elements obtained results correspond to the finding done " as discussed elsewhere by S. Brita et al. [26]" .According to EDX report, the weight percentage of O and Zn were found to be 26.6 and 72.2 respectively which close to bulk ZnO weight and the atomic percent found to be 57.2 and 40.7 for O of Zn. The spectrum reveal that very small concentration of carbon appeared. The presence of carbon in the sample can be attributed to carbon adhesive tape.

XRD Analysis

Fig. 3 depicts the XRD diffractogram of the ZnO NPs. The XRD patterns of the prepared samples match with the stander (ICSD card No. 067454). ZnO crystal have been grown with hexagonal phase, wurtzite structure. The calculated lattice parameters are a = 0.3249 nm, b = 0.5206 nm and their ratio (c/a = 1.601) are

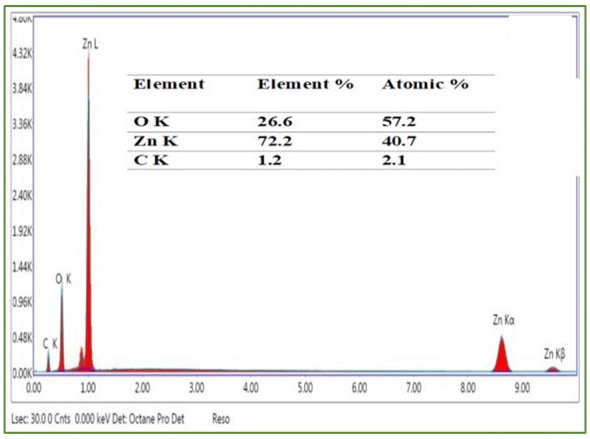

Fig. 2. EDX pattern of ZnO NPs.

matched with the reported result by Xiaofeng Zhou et al [27]. The structural parameters of ZnO NPs depicted in the inset in Fig.3. Experimental XRD calculation is in good agreement with reported with the result reported by "as discussed by H. Zayed et al [20]". No other phases have been observed, which further confirmed the formation of single phase ZnO. This diffraction peaks are significantly broadened due to the small size of the NPs [10]. The sharpness of diffraction peaks indicates to the good crystallinity. The average crystallite size of the sample was estimated from the broadening of the highest intensity peak (101) plane using Debye-Scherrer's equation[10,26].

where, D is the average crystallite size in nm, k is the particle shape factor (k = 0.9 for spherical particle), λ is the Cu K_α X-ray wavelength (0.15418 nm), β is the full width at half maximum (FWHM) of most intense peak corresponding to (101) plan and θ is the Bragg angle corresponding to the same plane which obtained from the diffraction angle (2θ). The calculated average crystallite size of ZnO NPs is obtained about 27.93 nm.

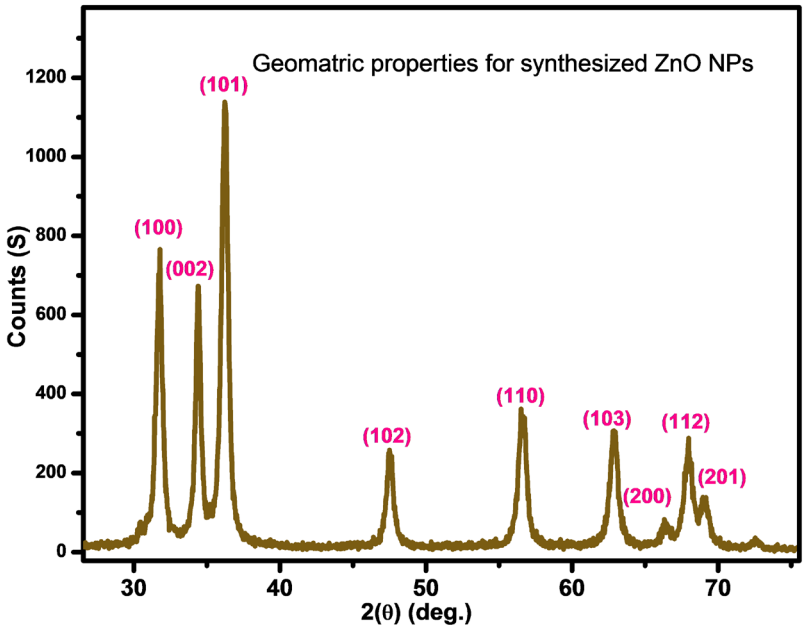

Fig. 3. X-ray diffraction pattern of ZnO.

HRTEM Analysis

The study of the surface morphology of the ZnO has been carried out by HRTEM. Fig.4. depicts the HRTEM (a) micrograph image, (b) diffraction patterns (c) selected electron diffraction area, and (d) crystallite size histogram. As shown in Fig.4. ZnO NPs has good crystalline, spherical and uniform with average particle size about 25.3 nm which is very closed to the estimated particle size about 27.93 nm from the XRD pattern. The spacing between the adjacent lattice planes (d_{hkl}) of ZnO NPs was measured from the bright field SAED patterns about 0.246 nm which is matched with the calculation results from XRD and corresponded to the (101) plane of ZnO.

UV–Vis optical absorbance and band gap

Fig. 5. illustrates the typical UV-Vis absorption spectrum of ZnO NPs in the wavelength range 300–800 nm. The ZnO NPs powder was ultrasonically dispersed in pure ethanol. In general, the UV absorption is related to the electronic transition from filled valence bands to empty conduction bands [1].

The spectrum reveals a characteristic absorption peak of ZnO at λ_{max} of 366.04 nm consistent with the bulk band gap of ZnO [27]. Optical energy gap can be estimated from, the intercept of linear portion of the curve on x-axis represented by energy (hv). In addition, the inset in Fig. 5 reveals that, the estimated optical energy gaps was about 3.12 eV, this value matches with previous work [5].

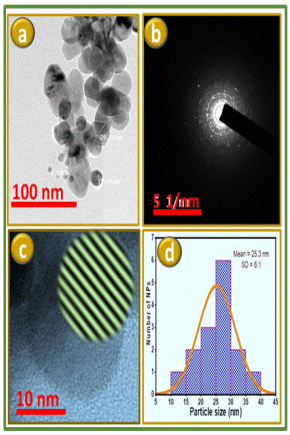

Fig. 4. HR-TEM micrograph image of ZnO NPs, (a) micrograph image, (b) diffraction pattern, (c) selected electron diffraction area (SAED), r = 5 (1/nm), and (d) crystallite size histogram.

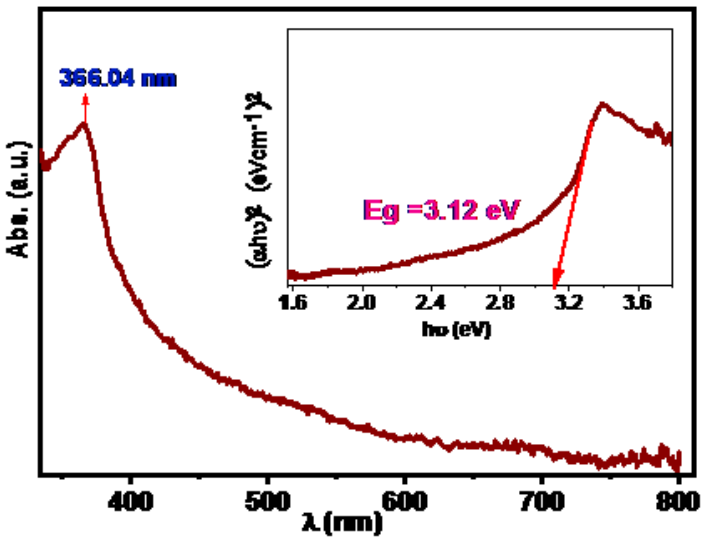

Fig. 5. Absorption spectra of ZnO NPs using ethanol as a solvent.

PL spectra analysis

PL technique is considered a good optical technique for analytical electron transitions between high and low energy levels. Also, it can be used to expect of the imperfections, impurities and defects in the synthesized materials. In some literatures the authors used PL spectroscopy to estimate the optical energy gap (26). Fig. 6 shows photoluminescence spectra (PL) from synthesized ZnO NPs at room temperature over wavelength from 300 to 800 nm, where the excitation wavelength about 320 nm emitted from a xenon lamp. PL spectra reveals four main characteristic intense peaks. The emission spectra are analyzed by fitting with multiple Gaussian curves. The photoluminescence emission spectra (PLES) is understood by de-convolution consisting of eight peaks as shown in Fig. 6. Bandwidths, relative intensities and band positions in individual energy bands of the observed emitted light in ZnO NPs are illustrated in Table 1. The PLES of ZnO NPs typically shows a linear emission in the Near-Ultraviolet range (NUVR) (originating as a result of exciton mechanism) and in the visible region which is attributed to defects in ZnO NPs [18]. The PLES of ZnO in visible region is attributed to the interior energy traps or defects present within the bandgap such as interstitials, imperfections, vacancies, impurities, anti-sites and principally, from the various oxygen vacancies [25]. The main features of the PLES of ZnO NPs can be classified into two regions: NUVR and visible. For the emission of NUVR region, the emission peaks centered at 348.7 nm (3.6 eV) and 383.6 nm (3.2 eV) which can be subjected to the near band edge (NBE) emission due to the radiative recombination of free excitons through an exciton–exciton collision process [29]. The near band emission from the ZnO nanocrystals, strongly, indicates the presence of $Zn(OH)_2$ [30]. In the visible region, the PLES can be divided into three categories: violet-blue (V-B), blue-green (B-G) and orange-red (O-R). The V-B emission can be decomposed into two peaks centered at 407nm (3.1 eV) and 429.2 nm (2.9 eV). VB emission peaks are assigned to the transition of electron from the bottom (donor) of conduction band to the energy level of Zn vacancy (V_{Zn}), which refers that the ZnO NPs is n-type semiconductors [31]. For the (B-G) emission, it consists of two peaks centered at 454.2 nm (2.7 eV) and 497.2 nm (2.5 eV), which caused by the transition of electrons from conduction band edge to the interior energy traps (IETs) complex [32]. The (O-R) centered at (□600–760) emission can be disbanded into two peaks centered at 629.3 nm (2 eV) and 647.3 nm (1.9 eV). is attributed to deep interstitial and vacancies of oxygen (O_i and V_o), respectively, in ZnO NPs [30,33].

Photoelectrical measurements

The main solar cell photovoltaic parameters are open circuit voltage (V_{OC}), short circuit current density (J_{SC}), maximum voltage (V_m), maximum current density (J_m), maximum power point (P_m), fill factor (FF), and photon to electric energy conversion efficiency (η). Fig. 7 illustrates the characteristics curves for the DSSCs sensitized

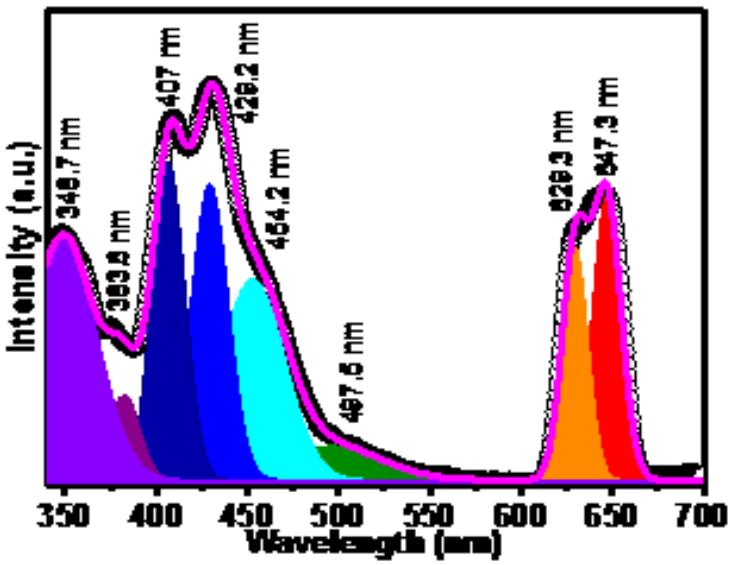

Fig. 6. A deconvolution of the photoluminescence spectrum emission into eight bands in ZnONPs.

with different concentration of Rhodamine B (RB). All J-V curves are found to have the same shape of diode's characteristic curve. The photovoltaic parameters for the fabricated DSSCs of ZnO NPs using different photosensitizer concentration are listed in Table 2. As seen in Table 2. The V_{OC} ranged from 0.364 to 0.436 V for the DSSC sensitized with 0.1 and 0.7 mM of RB, respectively. In addition, the J_{SC} varied from 0.06 to 2.62 $mAcm^{-2}$ for the DSSC sensitized with 0.1 and 0.7 mM of RB respectively. The highest J_{SC} was obtained for the DSSC sensitized with 0.7 mM of RB and the lowest J_{SC} was obtained for the DSSC sensitized with 0.1 mM of RB. The fill factor (FF) of the fabricated cells changed from 30.1 to 50.7%. In general, as the concentration of (RB) solution was increased, the exhibits photon to electric energy conversion efficiency increased up to 0.7 mM which is the optimum concentration, gives the best efficiency about 0.58 %. The dye concentration required for an optimal efficiency to be attained is directly related to the concentration of (RB) dye, and these results are consistent with aggregation and precipitation of dye molecules onto the photoelectrode surface when the concentration of (RB) is higher than 0.7 mM. In addition, the power against voltage is illustrated in the inset in Fig. 7.

TABLE 1. Bandwidths, relative intensities and Band positions in individual energy bands of the observed emitted light in ZnO.

Peak #	FWHM (nm)	I_p (a.u)	λ (nm)	Energy (eV)
Peak (I)	43.1	2638	348.7	3.6
Peak (II)	42.2	957	383.6	3.2
Peak (III)	21.2	3394	407	3.1
Peak (IV)	24.1	3162	429.2	2.9
Peak (V)	41.6	2192	454.2	2.7
Peak (VI)	63.4	434	497.2	2.5
Peak (VII)	16.7	2525	629.3	2.0
Peak VIII)	18.5	3050	647.3	1.9

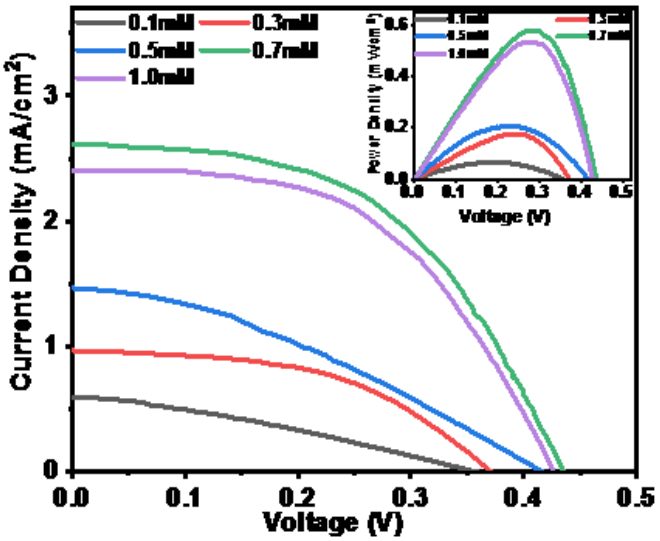

Fig. 7. J-V characteristics curves for the DSSCs based on ZnO NPs. Samples sensitized by different conc. of RB.

TABLE 2. Photovoltaic parameters for the DSSCs of ZnO NPs using different photosensitizer concentration

Dye Conc. (mM)	J_{sc} ($mAcm^{-2}$)	V_{oc} (V)	J_m ($mAcm^{-2}$)	V_m (V)	FF %	η %
0.10	0.60	0.36	0.34	0.19	30.11	0.07
0.32	0.96	0.37	0.72	0.24	49.20	0.18
0.50	1.45	0.42	0.92	0.23	34.65	0.21
0.70	2.62	0.44	1.97	0.29	48.65	0.58
1.00	2.41	0.43	2.01	0.26	51.74	0.53

Dye absorption spectrum

Fig. 8 illustrates the absorption spectrum of the RB dissolved in ethanol and adsorbed on a ZnO nonporous thin film. For the absorption spectrum of RB adsorbed on a ZnO thin film, absorption intensity due to the dimer increased compared to that in ethanol, indicating that the dimer of RB is formed on the ZnO surface. The absorption spectrum of RB adsorbed on ZnO film is broader compared to that in ethanol solution. In addition, the inset in Fig. 8. reveals that the shoulder which is attributed to the absorption of a dimer [34]. The onset of absorption is shifted from 443.55 to 551.32 nm. This can be explained by a change in the energy levels of highest occupied molecular orbital (HOMO) and lowest unoccupied molecular orbital (LUMO) of RB compared to those in solution, due to the interaction between RB molecules and the ZnO film[34, 35].

Transient open circuit voltage decay measurement

The transient open circuit photovoltage (TOCVD) technique has been employed as suitable method to investigate the electron lifetime (τ_n) and the electron recombination velocity (K_{rec}) in DSSC and can provide some quantitative information on the electron recombination velocity in DSSC. In order to conduct the TOCVD measurement, the sample was illuminated for two minutes to be equilibrium between electron injection and electron recombination at the FTO surface. i.e. a steady-state voltage was obtained and V_{oc} was recorded. After that, subsequent decay of photovoltage due to turning off the light source. The decay of the photovoltage reflects the decrease of the electron concentration at the FTO surface, which is primarily produced by the charge recombination. In other words, the recombination velocity of photoelectron is proportional to the response of the TOCVD[39]. A double exponential function (Fig. 9) is used as a powerful fitting function for the TOCVD data as depicted in Eq. (2) to extract the decay parameters [25].

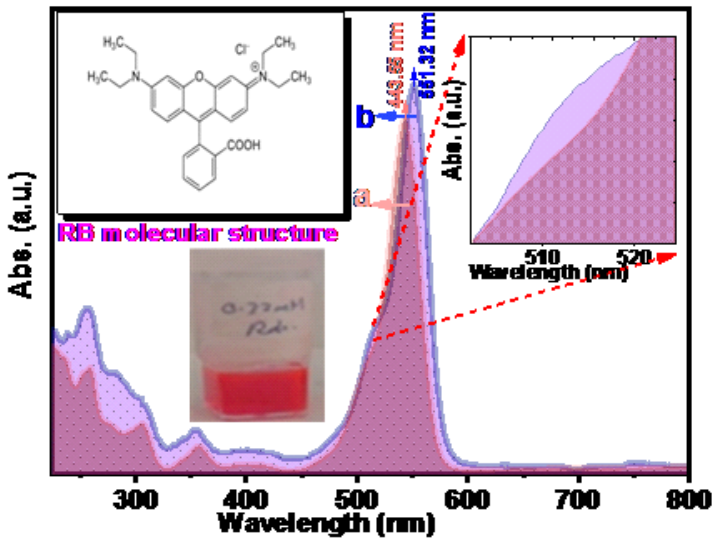

Fig . 8. The absorption spectrum of RB (a) free dye, (b) adsorbed on ZnO semiconductor layer dissolved in absolute ethanol.

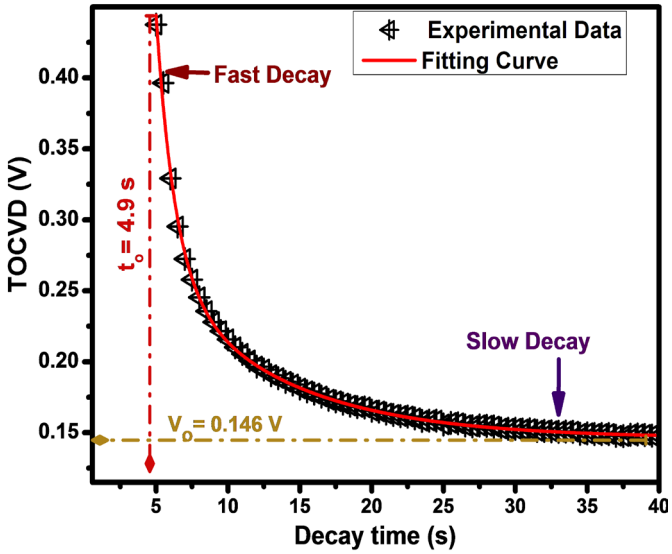

Fig. 9. Transient open circuit voltage V_{oc} decay of the cells sensitized RB. experimental data are shown in dotted lines and the fittings are presented in solid line

where, V_o is the offset of the $V_{oc.}$ The amplitudes of Voc for fast and slow curves are V_1 and V_2, respectively; t is the decay time and t_o is the center of the fitting curve. The decay time constant (lifetime) for fast curve and slow curve are τ_1 and τ_2 respectively. For the right-hand side of Eq. (2): The second term describes the fast decay and the third term describes the slow decay. All extracted decay parameters of the TOCPV are listed below in Table 3.

From the TOCVD testing, the electron lifetime (τ_n) is determined by the reciprocal of the first derivative of the decay curves normalized by the thermal voltage (V_t), using Eq. (3)

TABLE 3. The decay parameters of the TOCPV.

Decay parameters	V_o (V)	t_o (s)	Fast Decay		Slow Decay		τ_n (s)	k_{rec} $(s)^{-1}$	R^2
			V_1 (V)	τ_1 (s)	V_2 (V)	τ_2 (s)			
0.7mM RB	0.146	4.954	0.190	1.315	0.115	8.517	9.832	0.104	0.998

Where T is the temperature in Kelvin, K_B is the Boltzmann constant, and q is the elementary electron charge. Let which equal 0.026 V at room temperature. By differentiation of Eq. (2) with respect to (t) and substitution into Eq. (3)

Fig. 10. illustrates the electron lifetime as a function of V_{oc} for ZnO film. The shape of the TOCVD curve for ZnO film is match with "C. Gao et al [37]". The depression of the first region of the curve at around 0.27 V reflects the presence of recombination of electrons with the electrolyte through tunneling (surface trap states), while the strength of second linear region indicates that the high rate of recombination [38].

Conclusion

We have successfully synthesized ZnO Nps prepared by hydrothermal technique using zinc acetate dihydrate as a row material and aqueous solution of NaOH as precipitation agent; XRD pattern of ZnO clearly shows synthesized ZnO was wurtzite hexagonal structure. HRTEM investigation depicts that formation of spherical particles of 25.3 nm average particle size (D) which closes to XRD results. ZnO NPs shows an UV absorption intense peak at 366.04 nm corresponds to optical band gap of 3.13 eV. In addition, dye-sensitized solar cells (DSSCs) were dyed using (RB) dissolved in absolute

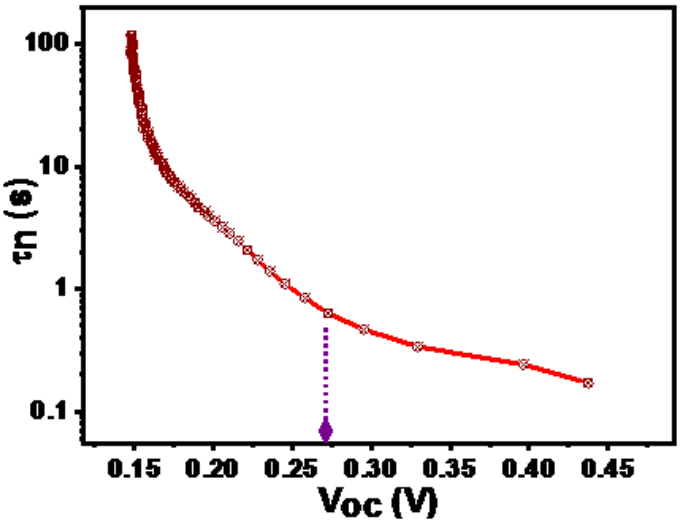

Fig. 10. Electron lifetime (τn) as a function of the open circuit voltage (Voc) of DSSC

ethanol with different concentration as sensitizers for nanocrystalline ZnO photoelectrodes. It is found that the best concentration of RB for the best performance among the tested dyes was 0.7 mM where the conversion efficiency of the cell reached 0.58%. Electron lifetime constants (τ_n) in DSSC was derived from Open-circuit voltage decay (TOCVD) which were about 1.315 and 8.517 s for fast and slow decay respectively**.**

References

1. Ibrahim A.M.,. Abd El-Latif M.M. and Gohr MSh.; Water/Alcohol Mediated Preparation of ZnO Hollow Sphere, *Egypt. J. Chem.* **58**(4), 475-484 (2015).

2. Mwafy E.A., Dawy M., Abouelsayed A., Elsabbagh I. A. and Elfass M.M.; Synthesis and Characterization of Multi-Walled Carbon Nanotubes Decorated ZnO Nanocomposite, *Egypt. J. Chem.* **59**(6), 1061-1068 (2016).

3. Rai P., Kim S.-G. and Yu Y.-T.; Microwave assisted synthesis of flower-like ZnO and effect of annealing atmosphere on its photoluminescence property, *J. Mater. Sci-Mater El.* **23**(2), 344–348 (2012).

4. Hanna A.A., Mohamed W.A.A. and Galal H.R.; Preparation, characterization and Evaluation of Nano Zinc Oxides as Pigments, *Egypt. J. Chem.*, **57**(5), 423-433 (2014).

5. Musleh H., AlDahoudi N., Zayed H., Shaat S., Tamous H.M., Shurrab N., Issa A. and Asad J.; Synthesis and Characterization of ZnO Nanoparticles Using hydrothermal and sol-Gel Techniques for Dye-Sensitized Solar Cells, *J. Univ. Babylon Eng. Sci.* **26**(9), 256-267 (2018).

6. Zhang Y., Nayak T.R., Hong H. and Cai W.; Biomedical applications of zinc oxide nanomaterials, *Curr Mol Med.* **13**(10), 1633–1645 (2013).

7. Ramadan M.A., Nassar S.H., Montaser A.S., El-Khatib E.M. and Abdel-Aziz M.S.; Synthesis of Nano-sized Zinc Oxide and Its Application for Cellulosic Textiles, *Egypt. J. Chem.*, **59**(4), 523-535 (2016).

8. Carcia P., McLean R., Reilly M. and Nunes Jr G.; Transparent ZnO thin-film transistor fabricated by rf magnetron sputtering, *Appl. Phys. Lett.* **82**, 1117-1119 (2003).

9. Thareja R. and Shukla S.; Synthesis and characterization of zinc oxide nanoparticles by laser ablation of zinc in liquid, *Appl. Surf. Sci.* **253**(22), 8889-8895 (2007).

10. Hammad T.M., Salem J.K. and Harrison R.G.; The influence of annealing temperature on the structure, morphologies and optical properties of ZnO nanoparticles, *Superlattice Microst.* **47**(2), 335-340 (2010).

11. Al Dahoudi N., Shaat S., Shurrab N., Issa A., Musleh H., Asaad J. and Zayed H.; Influence of Metal Ion Doping of zinc oxide photoanode on the efficiency of dye sensitized solar cell, *IUG Journal of Natural Studies,* (Special Issue) The Sixth International Conference on Science & Development (2017).

12. Meng F., Yin J., Duan Y.-Q., Yuan Z.-H. and Bie

L.-J.; Co-precipitation synthesis and gas-sensing properties of ZnO hollow sphere with porous shell, *Sensor. Actuat. B-Chem,* **156**(2), 703-708 (2011).

13. Shaat S.K.K., Musleh H., Zayed H., Tamous H., Issa A., Shurrab N., Asad J., Mousa A., Abu-Shawish M. and AlDahoudi N.; Solution combustion-derived ZnO nanoparticles for photoanode of solar cells, *Mater. Sci. Eng. B-Adv,* **241**, 75-81 (2019).

14. Fardood S.T., Ramazani A., Moradi S. and Asiabi P.A.; Green synthesis of zinc oxide nanoparticles using arabic gum and photocatalytic degradation of direct blue 129 dye under visible light, *J. Mater. Sci: Mater. Electron.* **28**(18), 13596-13601 (2017).

15. Rana S.B.; Influence of CTAB assisted capping on the structural and optical properties of ZnO nanoparticles, *J. Mater. Sci: Mater. Electron.* **28**(18), 13787-13796 (2017).

16. Hosono E., Fujihara S., Kimura T. and Imai H.; Non-basic solution routes to prepare ZnO nanoparticles, *J. Sol-Gel Sci. Techn.* **29**(2), 71–79 (2004).

17. Çopuroğlu M., Koh L.H.K., O'Brien S. and Crean G.M.; Comparative characterisation of zinc oxide thin films prepared from zinc acetate with or without water of hydration via the sol–gel method, *J. Sol-Gel Sci. Techn.* **52**, 432–438 (2009).

18. Li F., Ding Y., Gao P., Xin X. and Wang Z.L.; Single crystal hexagonal disks and rings of ZnO: low temperature, large scale synthesis and growth mechanism, *Angew. Chem. Int. Edit.* **43**(39) 5238-5242 (2004).

19. Singh N. and Haque F.Z.; Synthesis of zinc oxide nanoparticles with different pH by aqueous solution growth technique, *Optik*, **127**(1), 174-177 (2016).

20. Zayed H., Musleh H., Shaat S., Shurrab N., Asaad J. and AlDahoudi N.; Synthesis of zinc oxide nanoparticles at different aging time for low cost dye sensitized solar cells, *Journal of Scientific Research in Science*, **34**(1), 275-286 (2017).

21. Ba-Abbad M.M., Chai P.V., Takriff M.S., Benamor A. and Mohammad A.W.; Optimization of nickel oxide nanoparticle synthesis through the sol–gel method using Box–Behnken design, *Materials & Design,* **86**, 948-956 (2015).

22. Luo J., Lin J., Zhang N., Guo X., Zhang L., Hu Y., Lv Y., Zhu Y. and Liu X.; Eu and F co-doped ZnO-based transparent electrodes for organic and quantum dot light-emitting diodes, *J. Mater. Chem. C* **6**, 5542-5551 (2018).

23. Mote V., Purushotham Y. and Dole B.; Williamson-Hall analysis in estimation of lattice strain in nanometer-sized ZnO particles, *J. Theor. Appl. Phys. (2012)* **6**, 6 (2012).

24. He L., Tong Z., Wang Z., Chen M., Huang N. and Zhang W.; Effects of calcination temperature and heating rate on the photocatalytic properties of ZnO prepared by pyrolysis, *J. Colloid. Interf. Sci.* **509**, 448-456 (2018).

25. Shaat S., Zayed H., Musleh H., Shurrab N., Issa A., Asad J. and Al Dahoudi N.; Inexpensive organic dyes-sensitized zinc oxide nanoparticles photoanode for solar cells devices, *J. of Photonics for Energy* **7**(2), 025504 (2017).

26. El Mogy S.A., Youssef R.S. and Abd El Megeed A.A.; Processing of Polyurethane Nanocomposite Reinforced with nanosized Zinc Oxide: Effect on Mechanical and Acoustic Properties, *Egypt. J. Chem.* **62**(2), 333-341 (2019).

27. Zhou X., Xie Y., Mi H., Ma J., Yang J. and Cheng J.; Comparative study of two methods for the synthesis of $CuBi_2O_4$ particles and their application in ZnO-based dye-sensitized solar cells, *J. Mater. Sci-Mater El.*, **28**(18), 13437–13444 (2017).

28. Kundu T.K., Karak N., Barik P. and Saha S.; Optical properties of ZnO nanoparticles prepared by chemical method using poly (vinyl alcohol) (PVA) as capping agent, *International Journal of Soft Computing and Engineering* **1**(Issue-NCRAMT2011), 19-24 (2011).

29. Rodnyi P. and Khodyuk I.; Optical and luminescence properties of zinc oxide (Review), *Opt. Spectrosc.* **111(5)**, 776–785 (2011).

30. Patwari G., Bodo B., Singha R. and Kalita P.; Photoluminescence Studies of H_2O_2 Treated Chemically Synthesized ZnO Nanostructures, *Res. J. Chem. Sci.* **3**(9), 45-50 (2013).

31. Suhail A.M., Saleh W.R., Ibrahim O.A. and Ibrahim R.K.; Synthesies of ZnO quantum dot by by self assemply method and ZnO nanorod by hydrothermal method, *International Journal of Advanced Technology in Engineering and Science* **3**(4), 172-182 (2015).

32. Karthikeyan T.P.B. and Mangaiyarkarasi K.; Optical properties of sol–gel synthesized calcium doped ZnO nanostructures, *Spectrochim Acta A Mol Biomol Spectrosc.* **82**(1), 97-101 (2011).

33. Brauchli S.Y., Constable E.C. and Housecroft C.E.; Concentration effects on the performance of bis (dimine) copper (I) dyes in dye-sensitized solar cells, *Dyes Pigments* **113**, 447-450 (2015).

34. Hara K., Horiguchi T., Kinoshita T., Sayama K., Sugihara H. and Arakawa H.; Highly efficient photon-to-electron conversion with mercurochrome-sensitized nanoporous oxide semiconductor solar cells, *Sol. Energ. Mat. Sol. C.* **64**(2), 115-134 (2000).

35. Rohatgi K. and Singhal G.; Nature of bonding in dye aggregates, *J. Phys. Chem.* **70**(6), 1695–1701 (1966).

36. Fabregat-Santiago F., García-Cañadas J., Palomares E., Clifford J.N., Haque S.A. and Durrant J.R.; The origin of slow electron recombination processes in dye-sensitized solar cells with alumina barrier coatings, *J. Appl. Phys.* **96**(11), 6903-6907 (2004).

37. Gao C., Li X., Lu B., Chen L., Wang Y. and Teng F.; A facile method to prepare SnO 2 nanotubes for use in efficient SnO_2-TiO_2 core-shell dye-sensitized solar cells, *Nanoscale,* **4**(11), 3475-3481 (2012).

38. Archana P., Jose R., Vijila C. and Ramakrishna S.; Improved electron diffusion coefficient in electrospun TiO_2 nanowires, *J. Phys. Chem. C.* **113**(52), 21538–21542 (2009).

تحسين أداء الخلايا الشمسية الصبغية باستخدام جسيمات نانومترية من أكسيد الزنك وصبغة الرودامين ب كمتحسس للضوء

حسام مصلح[١،٢] ، حمدية عبد الحميد زايد[٢] ، سامي شعث[٣]، أمل الكحلوت[١]،
حسن طموس[٥] ، أحمد عيسي[٤]، جهاد اسعد[١] و ناجي الداهودي[١]

[١] جامعة الازهر- قسم الفيزياء-غزة - فلسطين
[٢] كلية البنات للاداب والعلوم والتربية - جامعة عين شمس - القاهرة - مصر
[٣] الجامعة الاسلامية- قسم الفيزياء -غزة - فلسطين
[٤] جامعة الازهر - قسم الكيمياء - غزة - فلسطين
[٥] جامعة الازهر - كلية الهندسة -غزة - فلسطين

في هذا البحث تم تخليق جسيمات نانومترية من أكسيد الزنك النقي باستخدام طريقة الهيدروثيرمال. تم استخدام اسيتات الزنك كمادة أولية ومحلول قلوي من هيدروكسيد الصوديوم كمحلول لازم للترسيب قياسات حيود الاشعة السينية بينت ان المادة المحضرة هي أكسيد الزنك بلورة سداسية من النوع وريدزايت قياسات المجهر الالكتروني النافذ بينت ان الجسيمات المخلقة كروية متوسط حجمها ٣,٥٢ نانومتر وهذه القيمة متوافقة مع قياسات حيود الاشعة السينية. القياسات الضوئية بينت ان اعلي امتصاص كان عند ٤٠,٦٦٣ نانومتر وان فجوة الطاقة الضوئية كانت تقريبا ٣١,٣ الكترون فولت. القياسات الكهربية للخلايا الشمسية المحضرة باستخدام تراكيز مختلفة من صبغة الرودامين ب بينت ان افضل تركيز كان ٧,٠Mm حيث كانت الكفاءة الكهربية للخلية تساوي ٨٥,٠٪ . بينت قياسات منحني الاضمحلال للجهد ان قيم (nτ) هي ٥١٣,١ ثانية و ٧١٥,٨ ثانية للاضمحلال السريع والبطيء في المنحني علي الترتيب.